Ecophysiological Study of *Paraburkholderia* sp. Strain 1N under Soil Solution Conditions: Dynamic Substrate Preferences and Characterization of Carbon Use Efficiency

K. Taylor Cyle,[a] Annaleise R. Klein,[b] Ludmilla Aristilde,[b,c] Carmen Enid Martínez[a]

aSoil and Crop Sciences, School of Integrative Plant Science, College of Agriculture and Life Sciences, Cornell University, Ithaca, New York, USA
bDepartment of Biological and Environmental Engineering, Cornell University, Ithaca, New York, USA
cDepartment of Civil and Environmental Engineering, McCormick School of Engineering and Applied Science, Northwestern University, Evanston, Illinois, USA

ABSTRACT We used time-resolved metabolic footprinting, an important technical approach used to monitor changes in extracellular compound concentrations during microbial growth, to study the order of substrate utilization (i.e., substrate preferences) and kinetics of a fast-growing soil isolate, *Paraburkholderia* sp. strain 1N. The growth of *Paraburkholderia* sp. 1N was monitored under aerobic conditions in a soil-extracted solubilized organic matter medium, representing a realistic diversity of available substrates and gradient of initial concentrations. We combined multiple analytical approaches to track over 150 compounds in the medium and complemented this with bulk carbon and nitrogen measurements, allowing estimates of carbon use efficiency throughout the growth curve. Targeted methods allowed the quantification of common low-molecular-weight substrates: glucose, 20 amino acids, and 9 organic acids. All targeted compounds were depleted from the medium, and depletion followed a sigmoidal curve where sufficient data were available. Substrates were utilized in at least three distinct temporal clusters as *Paraburkholderia* sp. 1N produced biomass at a cumulative carbon use efficiency of 0.43. The two substrates with highest initial concentrations, glucose and valine, exhibited longer usage windows, at higher biomass-normalized rates, and later in the growth curve. Contrary to hypotheses based on previous studies, we found no clear relationship between substrate nominal oxidation state of carbon (NOSC) or maximal growth rate and the order of substrate depletion. Under soil solution conditions, the growth of *Paraburkholderia* sp. 1N induced multiauxic substrate depletion patterns that could not be explained by the traditional paradigm of catabolite repression.

IMPORTANCE Exometabolomic footprinting methods have the capability to provide time-resolved observations of the uptake and release of hundreds of compounds during microbial growth. Of particular interest is microbial phenotyping under environmentally relevant soil conditions, consisting of relatively low concentrations and modeling pulse input events. Here, we show that growth of a bacterial soil isolate, *Paraburkholderia* sp. 1N, on a dilute soil extract resulted in a multiauxic metabolic response, characterized by discrete temporal clusters of substrate depletion and metabolite production. Our data did not support the hypothesis that compounds with lower energy content are used preferentially, as each cluster contained compounds with a range of nominal oxidation states of carbon. These new findings with *Paraburkholderia* sp. 1N, which belongs to a metabolically diverse genus, provide insights on ecological strategies employed by aerobic heterotrophs competing for low-molecular-weight substrates in soil solution.

KEYWORDS ecophysiology, *Paraburkholderia*, nominal oxidation state of carbon, time-resolved metabolic footprinting, carbon use efficiency

Low-molecular-weight (LMW) compounds in soil solution comprise a small amount of total soil carbon yet represent an important carbon pool at the interface between the decomposition of larger residues and subsequent assimilation by the soil microbial community (1). The LMW C pool is typically less than 10% of soil solution C and totals to 1 to 2 g of C m^{-2} down to a meter depth in typical forest soils (2). Because of their small compound size (<1 kDa) and the presence of specific and nonspecific membrane transport systems in microbial cells, LMW compounds are rapidly assimilated and mineralized by the microbial community (3). The composition of the LMW fraction of soil solution reflects common precursors and intermediates found in the metabolism of plant and microbial cells (4). These compounds, primarily sugars, amino acids, and organic acids, are maintained at low concentrations by a balance of microbial uptake and a constant supply from metabolite release, cell death, root exudation, depolymerization, and downward movement of soil solution (5). Estimates of half-lives of specific compounds within this class vary from less than an hour to more than 7 days depending on the soil horizon being investigated (6–8). Though rapidly cycled, these compounds are thought to disproportionately make up persistent C and N pools after transformation (1) and are increasingly being represented in finer resolution in microbially explicit models to predict stabilization rates (9).

Compound uptake preferences and metabolic use efficiency (carbon use efficiency [CUE], synonymous with microbial growth yield) of LMW C and N is predetermined and regulated by the individual microbial cell (10) as well as influenced by environmental stoichiometric limitations (11) and the presence and availability of other organic substrates (12). A current question is whether we may determine first principles for the diverse metabolic potential inherent in the soil microbial community. Previous exometabolomic trials with bacteria and yeasts have shown almost no links between genetic or ecotype relatedness and substrate uptake patterns (13) to strong genotypic clustering or mixed clustering in relation to substrate uptake (14, 15). There is evidence for (16) and against (17) whether individual bacterial populations exhibit conserved uptake preferences when diverse resources are abundant. Quantitative stable isotope probing work on complex, *in situ* soil communities suggests that evolutionary background may be the main constraint on carbon assimilation (18). One relatively well-defined ecophysiological paradigm that appears to hold true for soil bacteria is the broad distinction between copiotrophic (*r*-selected) and oligotrophic (*K*-selected) life histories (19). In this framework, copiotroph populations have higher growth rates, are adapted to pulsed input events, and tend to exhibit inefficient conversion of LMW C into biomass (10). Our current capacity to model LMW C cycling in soil solution may be limited by our ability to define the predominant ecophysiological characteristics that govern heterotroph activity.

There is clear evidence from LMW tracer experiments in the field (20–22) and laboratory incubations (23–25) that oxidized compounds are taken up more rapidly by the microbial community, followed by a less efficient conversion of that C to biomass (lower CUE) in surficial soil horizons. These observations are often associated with an inferred relationship between the energetic content of a carbon substrate (12, 26) and its potential CUE. Generally, a compound with a higher nominal oxidation state (NOSC) will require more energy, in the form of reducing equivalents, to reduce the carbon to the oxidation state of the biomass being created (~ -0.2). In other words, growth on substrates with a NOSC above that of biomass (27) will reduce growth efficiency due to energy limitations, while substrates with a NOSC far below that of biomass will be carbon limited during growth (28). It is also possible that under mixed-substrate utilization, the more oxidized compound could be used primarily for energy generation alone (12). This may explain earlier and less efficient use of higher-NOSC compounds in these studies. It has been hypothesized that the relationship between NOSC and CUE may resemble a bell-shaped curve centered around the NOSC of biomass (29). However, under aerobic conditions, a more likely relationship is a linear increase to a theoretical maximum with increasing energetic content (lower NOSC) (30).

Relationships between compound identity, uptake, and CUE are not as clear at the

microbial population level. Substrate preferences can be extremely divergent, even across similar fast-growing isolates (31). A traditional view is that these fast-growing organisms, which are considered copiotrophs, should stagger uptake based on potential maximal growth rate on that substrate (19). This phenomenon, known as catabolite repression, is the classic paradigm of microbial substrate selection and often exhibits diauxic growth patterns (32, 33).

Much of the theoretical underpinning for the hypotheses that higher-NOSC compounds are more readily assimilated or those that support catabolite repression are based on simplified, minimal media (34). The NOSC framework, though field tested, is built upon single-carbon-source-culturing trials (30), and deviations can be observed under even simple mixed-substrate-culturing conditions (12). There is also an assortment of observations showing simultaneous use of substrates that provide medium or low maximum growth rates when low-concentration, mixed-substrate media are used (35). It is imperative that appropriate media mimicking the relevant ecological niches be used to develop relationships between compound characteristics and C utilization (36). Time-resolved metabolic footprinting provides an avenue for addressing these concerns (17). This approach uses sigmoidal model fits to define the midpoint of substrate depletion from the media (t_{50}) and parse out substrate preferences during microbial growth. It has been used in conjunction with both natural (37–39) and defined, complex media (40) and has shown the ability to link isolate exometabolite profiling with *in situ* community function (41).

In this work, we utilized time-resolved exometabolomic footprinting to profile substrate preferences and CUE of the fast-growing soil bacterium *Paraburkholderia* sp. strain 1N (42). *Paraburkholderia* is a relatively newly defined genus created from the subdivision of *Burkholderia* and predominantly isolated from bulk soil and the rhizosphere or found as endophytes (43–45). This organism has been found to preferentially respond to additions of phenolics and drive priming in forested soils (46). *Paraburkholderia* sp. 1N was isolated using an undefined, complex growth medium referred to as soil-extracted solubilized organic matter (SESOM) (47) derived from an organic rich surface horizon in a hemlock-hardwood stand. SESOM was used to recreate conditions encountered in soil solution following rainwater infiltration and residence in a surficial forest soil when fast-growing populations are most active. The depletion of naturally occurring organic substrates as well as appearance of metabolites was monitored in batch study using liquid chromatography (LC) coupled with high-resolution mass spectrometry (HRMS) as well as ¹H nuclear magnetic resonance (NMR) analyses. Our aim was to phenotype this fast-growing soil microorganism under realistic, pulsed input conditions. We tested for relationships between substrate chemical parameters (NOSC, initial concentration) and microbial preferences (t_{50}) and depletion rates, as well as explored potential links between the aforementioned parameters and CUE.

RESULTS

Isolation and genomic characterization. The forest soil isolate *Paraburkholderia* sp. 1N was isolated on soil-extracted solubilized organic matter (SESOM) and classified to the genus *Paraburkholderia* (see Fig. S2 in the supplemental material) (42). Draft genome size was measured to be 11.1 Mb, containing 353 contigs, with a GC content of 60.6%. The annotated draft genome was found to contain 11,964 coding genes with 4,045 distinct functions. Only 3,704 genes could be matched with SEED annotation ontology. The largest portions of annotated genes are assigned functions that fall within carbohydrate metabolism ($n = 1,039$), amino acid metabolism ($n = 666$), and metabolism of aromatic compounds ($n = 487$) (Fig. S3). The phosphoenolpyruvate protein of the phosphotransferase system (PTS), a type of phosphotransferase system implicated in well-studied carbon catabolite repression systems, is present (EC 2.7.3.9). Annotated ATP-binding cassette (ABC) transporters of interest include the presence of the branched-chain amino acid uptake systems (Liv, TC 3.A.1.4.1), an oligopeptide uptake system (Opp, TC 3.A.1.5.1), and a dipeptide system (Dpp, TC 3.A.1.5.2). Further characterization of this isolate can be found in the work of Wilhelm et al. (42).

TABLE 1 SESOM initial solution characteristics

Component	Value	Unit
pH	3.55	
EC	164	μS/cm
TOC	183.1	mg of C/liter
TN	11.3	mg of N/liter
NH_4^+	1.79	mg of N/liter
Ninhydrin-N	4.59	mg of N/liter
Reducing sugars, C	30.7	mg of C/liter

SESOM provides a complex, realistic growth medium. SESOM was created from the organic (Oa) horizon of the hemlock-dominated stand, and initial characterization was conducted using a range of analytical techniques. SESOM had a yellowish hue and was acidic (Table 1). Potassium was the major cationic component, with appreciable amounts of sodium, aluminum, and iron as well (Table S1). There was no detectable, dissolved inorganic carbon at this pH, and therefore, the entirety of measured solution carbon was organic. The solution had an observed C/N ratio of 16.4. Approximately 16% of solution nitrogen (TN) was in the form of NH_4^+, while 41% was found to be in the ninhydrin-reactive pool and was considered to be predominantly in the form of amino acids. The remaining 43% was uncharacterized but organic in nature. Reducing sugars accounted for 16.5% of total organic carbon (TOC) in the solution. Specific LMW compounds of interest were quantified using two different targeted LC-HRMS and ^{1}H NMR measurements (Table 2; see also Materials and Methods). In total, compounds targeted using LC-HRMS and ^{1}H NMR and colorimetric methods accounted for 19.5% of TOC and 39.9% of TN. Many additional compounds could be putatively identified using untargeted approaches but could not be quantified. Glucose is the dominant sugar present and the only sugar estimate that could be reliably made from ^{1}H NMR spectra (Table 2 and Fig. S1). Valine, alanine, and glutamate were the dominant amino acids present, while acetate, lactate, and gluconate were the predominant organic acids present out of those quantified (Table 2).

Paraburkholderia sp. 1N was grown aerobically in SESOM and growth rate (μ_{max}) was determined to be 0.17 h^{-1} (generation time = 4.1 h) using linear fitting during exponential growth (Fig. 1). During the course of growth, 51.8 mg of C/liter (28.3% of initial TOC) was assimilated and 32.5 mg of C/liter (17.7% of initial TOC and 62.8% of assimilated C) was lost from the culturing vessel entirely (Fig. 2). This amount was assumed to be predominantly respiratory CO_2 losses from the system (Fig. 2A, cumulative CO_2), though it could have contained small amounts of volatile organic carbon as well. Biomass production reached a mean plateau of 21.7 mg of C/liter at stationary phase. Reducing sugars could potentially explain a large portion of C assimilated from SESOM medium (up to 31% of total C assimilated [Table 2]). Similarly, nitrogen was assimilated from SESOM medium during growth (Fig. 2B). Initially, amino acid N concentrations decreased, followed by a switch to predominantly NH_4^+ before a return to amino acid N depletion as NH_4^+ concentrations dropped below detection (Fig. 2B). Approximately 6.7 mg of N/liter was removed from solution and incorporated in the biomass of *Paraburkholderia* sp. 1N. Total amino acid N (4.05 mg of N/liter) and total NH_4^+ N depletion (1.79 mg of N/liter) accounted for all but 0.86 mg of N/liter removed from solution, indicating a smaller contribution of alternative N sources to microbial uptake (Fig. 2B). There was no significant loss of N from the system.

Estimates of cumulative CUE show an increase through the growth curve to a plateau of 0.43 (Fig. 3). Instantaneous estimates were calculated over each measurement period to determine if higher instantaneous rates were achieved. A maximum of 0.54 was estimated over the 19- to 22-h portion of the experiment, which encompasses the inflection point of the growth curve. Instantaneous CUE rapidly declined after the inflection point as growth slowed and the population entered stationary phase.

Time-resolved exometabolomic footprinting provides information on compound depletion and appearance patterns. LC-HRMS and ^{1}H NMR were used for the

TABLE 2 Targeted substrate initial concentrations and depletion dynamics

Compound	Symbol	Units	Source[a]	Type[b]	Initial concn	a	o	t_{50}	w	%[c]	NOSC
Pyruvate	pyr	µM	M	1	0.37	0.37	0.00			0.03	0.67
α-Ketoglutarate	akg	µM	M	1	0.59	0.43	0.16			0.05	0.80
Ornithine	orn	µM	A	1	0.96	0.43	0.53			0.05	−0.40
Methionine	met	µM	A	1	1.03	0.75	0.28			0.09	−0.40
Phenylalanine	phe	µM	A	1	1.08	0.57	0.51			0.12	−0.33
Malate	mal	µM	M	1	1.21	0.93	0.28			0.09	1.00
Histidine	his	µM	A	1	1.65	1.27	0.37			0.18	0.67
Lysine	lys	µM	A	1	1.67	1.19	0.48			0.17	−0.67
Citrulline	cit	µM	A	1	2.24	1.57	0.67			0.36	−0.80
Arginine	arg	µM	A	1	3.00	2.70	0.31			0.38	0.33
2-Keto-D-gluconate	2kg	µM	M	1	3.20	3.04	0.16			0.42	0.67
Asparagine	asn	µM	A	1	4.24	4.24	0.00			0.39	1.00
Serine	ser	µM	A	1	6.00	6.00	0.00			0.42	0.67
Succinate	succ	µM	M	1	6.57	6.57	0.00			0.61	0.50
Glutamine	gln	µM	A	1	9.05	8.53	0.71			0.97	0.40
Aspartate	asp	µM	A	1	11.50	11.50	0.00			1.07	0.75
Gluconate	glucon	µM	M	1	17.63	17.26	0.37			2.37	0.33
Glutamate	glu	µM	A	1	54.92	54.92	0.00			6.23	0.40
Alanine	ala	µM	H	1	70.00	44.00	26.00			3.06	0.00
Acetate	ace	µM	H	1	95.60	72.53	23.07			3.37	0.00
Proline	pro	µM	A	2	0.83	0.43	0.40	16.29	0.57	0.05	−0.40
Isoleucine	ile	µM	M	2	1.94	1.92	0.02	16.79	0.99	0.27	−1.00
Leucine	leu	µM	M	2	9.55	9.51	0.04	16.93	0.52	1.33	−1.00
Tryptophan	trp	µM	A	2	0.62	0.62	0.00	17.06	0.19	0.16	−0.18
Tyrosine	tyr	µM	A	2	0.65	0.65	0.00	17.08	0.08	0.14	−0.22
Citrate	citr	µM	M	2	2.59	2.55	0.04	17.33	0.36	0.18	1.00
Lactate	lac	µM	H	2	24.94	7.34	17.60	17.90	1.09	0.65	0.00
Threonine	thr	µM	A	2	6.40	5.91	0.49	17.93	0.62	0.55	0.00
Ammonium	NH_4^+	mg N/liter	C	2	2.07	2.07	0.00	20.32	0.78		
Reducing sugars[d]		µM	C	2	430.42	248.35	182.07	20.42	1.47	31.29	0.00
Valine	val	µM	A	2	168.29	168.29	0.00	20.52	0.72	19.96	−0.80
Glucose	glc	µM	H	2	192.01	134.82	57.19	21.06	1.15	17.82	0.00
Unidentified	Unknown aromatic	AUC	H	2	1.00	0.62	0.38	21.82	0.14		

[a]"Source" refers to the analytical technique used (M, LC-HRMS-Metabo method; A, LC-HRMS-AA method; H, ¹H NMR; C, colorimetric).

[b]Type 1 refers to substrates depleted before the first sampling point, while type 2 substrates have been fit to a sigmoidal depletion curve: $y = \dfrac{a}{1+e^{\frac{x-t_{50}}{w}}} + o$

[c]Refers to percentage of total C assimilated (51.8 mg of C/liter) that could be attributable to the targeted substrate.

[d]Reducing sugars method includes glucose values.

direct quantification of 31 targeted compounds at each time point sampled during the growth of *Paraburkholderia* sp. 1N in SESOM (Table 2). Depletion patterns were analyzed by overlaying the t_{50} and 90% usage window of each substrate onto the growth curve of the organism (Fig. 4) (17, 31). Concentrations of all of the 31 targeted compounds decreased during the course of growth. It is important to note that the technique does not independently confirm the presence of these compounds intracellularly, and the terms depletion and usage are employed throughout this paper instead of uptake and assimilation. There is a possibility of extracellular transformation without uptake or even uptake without subsequent usage (38).

Substrate depletion from the media occurred in three distinct clusters, as determined by usage window plotting (Fig. 4) (17). The first cluster, containing 20 of the 31 substrates, occurred predominantly before the first sampling event and the substrate depletion pattern was either entirely or almost entirely missed, making them type 1 substrates (Fig. 4, inset, and Fig. S4; see Materials and Methods). The first cluster of compounds consisted of a mixture organic acids and amino acids (Table 2 and Fig. 4). There was a slightly higher abundance of compounds with NOSC greater than 0 in this earlier phase of depletion (Fig. 4, inset). The remaining 11 substrates were removed from the media during the sampling period and could be fit to a sigmoidal uptake curve (type 2 substrates [Fig. S5]). Type 2 substrates fell into two separate clusters of overlapping usage, one before the inflection point of growth and one occurring afterwards (Fig. 4). The second cluster contained mainly amino acids (proline, isoleu-
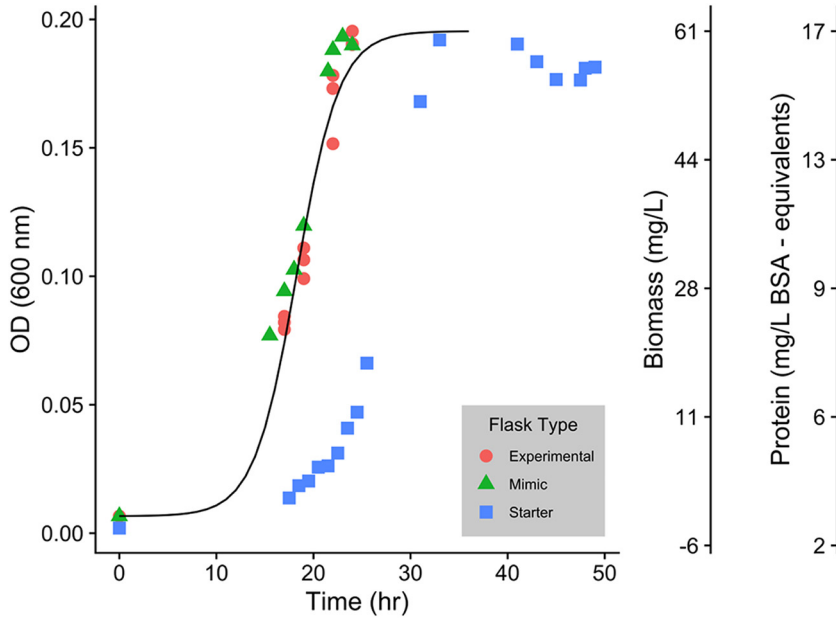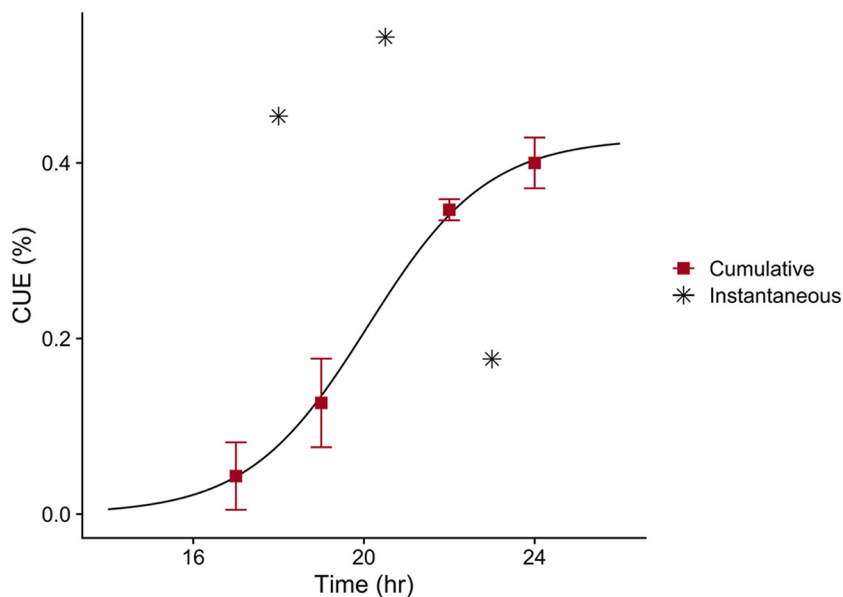
FIG 1 Growth curve of *Paraburkholderia* sp. 1N on SESOM. Data were collected from experimental replicates ($n = 3$), a mimic flask ($n = 1$), and a starter flask ($n = 1$) used in the experiment. The y axes display optical density measured photometrically at 600 nm as well as a biomass conversion (biomass [milligrams per liter] = 343.09 OD_{600} − 5.38) and cellular protein content (protein [milligrams per liter BSA equivalents] = 67.19 OD_{600} + 2.78). Biomass was measured only on experimental replicates via 0.2-μm filtration and protein content using a Bradford assay after cell lysis using dual analytical replicates. The starter flask was used for initial inoculation ($OD_{600} = 0.0658$) and is pictured to provide support for forcing the model fit.

cine, leucine, tryptophan, and tyrosine) as well as two organic acids (citrate and lactate) (Table 2 and Fig. S5). The third cluster consisted of glucose and valine disappearance as well as the removal of unidentified aromatic peaks (identified via ^{1}H NMR and assumed to be attributed to tannin-like molecules) coupled with NH_4^+ uptake (Fig. 4
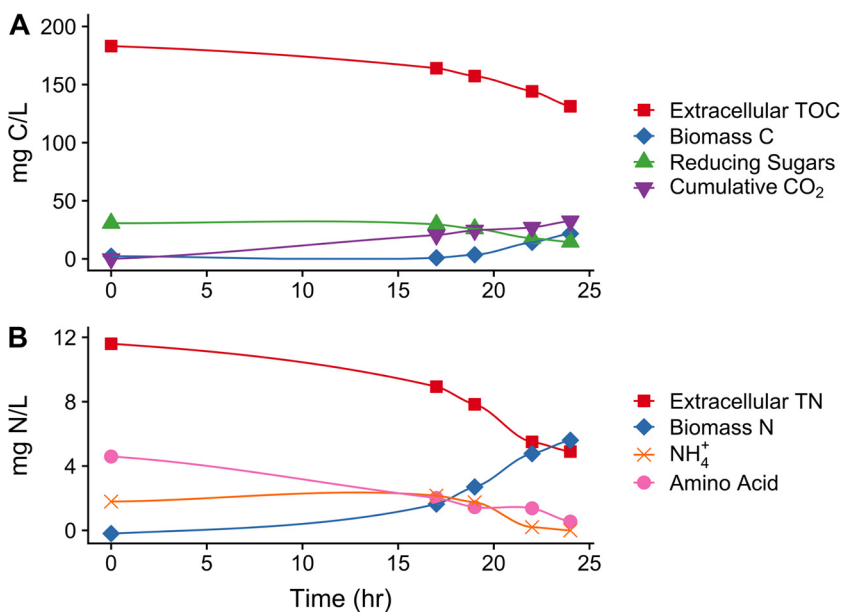
FIG 2 Carbon and nitrogen dynamics during *Paraburkholderia* sp. 1N growth on SESOM. Panel A displays changes to carbon pools, and panel B displays nitrogen pools. All points represent means ($n = 3$) with standard error bars (smaller than point size in all cases).

FIG 3 Carbon use efficiency (CUE) during microbial growth of *Paraburkholderia* sp. 1N on SESOM. All points represent means with standard error bars ($n = 3$). Instantaneous CUE was calculated from growth in between biomass sampling points, so estimated values are displayed at the center of the measurement period. A similar 4-point sigmoidal curve was fit for cumulative CUE, $y = \dfrac{a}{1+e^{\frac{-(x-t_{50})}{w}}} + o$, where $a = 0.43$, $t_{50} = 20.09$, $w = 1.40$, and $o = 0$.

and Fig. S5). Total reducing sugars had an earlier t_{50}, indicating that the multiple other, lower-concentration, sugars had a slightly earlier removal. This later cohort of compounds comprise the largest concentrations of available C and N in solution out of the substrates quantified. Targeted substrates, overall, represented 74.9% and 74.4% of total C and N depletion, respectively (Table 2).

An untargeted approach was then employed to look for compounds beyond those targeted previously. In total, 135 significant features were detected and the area under the curve was quantified. Of the 135 detected features, 99 decreased and 36 increased during the growth of *Paraburkholderia* sp. 1N (Fig. S6 to S12). Only 21 of the decreasing features could be fit using equation 2 in Materials and Methods (Fig. S7), and only 15 of increasing features could be fit with the modified version of the same equation (Fig. S11). A combined plot was used to visualize the depletion and appearance of these features (Fig. 5A). There was a clear distinction between the t_{50} of decreasing and increasing features, with the mean t_{50} of decreasing features occurring 2.4 h before that of the increasing features [two-sample $t(34) = -6.3742$; $P < 0.001$]. Compound appearance tended to occur over smaller intervals (90% usage window) than substrate depletion, with a 3.3-h-longer usage window estimate for decreasing features [Wilcoxon rank sum $W(34) = 279$; $P < 0.001$].

Inclusion of untargeted features show that *Paraburkholderia* sp. 1N exhibited metabolic diversity in the variety of compounds that could be depleted from SESOM media. Similar levels of superclass diversity were removed from the extracellular matrix as were transformed or released as metabolites or upon cell death ($n = 8$) (Fig. 5B and C). Alkaloids and phenylpropanoids and polyketides were only removed from SESOM media, and both superclasses showed late disappearance (Fig. 5B, type 4). Benzenoids and nucleosides, nucleotides, and analogues were only released into the SESOM media, and both superclass categories of compounds showed irregular appearance profiles (Fig. 5C, type 3). Of the untargeted features that could be fit to a sigmoidal usage pattern (Fig. 5B and C, type 2), similar ranges of superclasses were involved (lipids, organic acids, organic nitrogen compounds, organic oxygen compounds, and organoheterocyclic compounds).
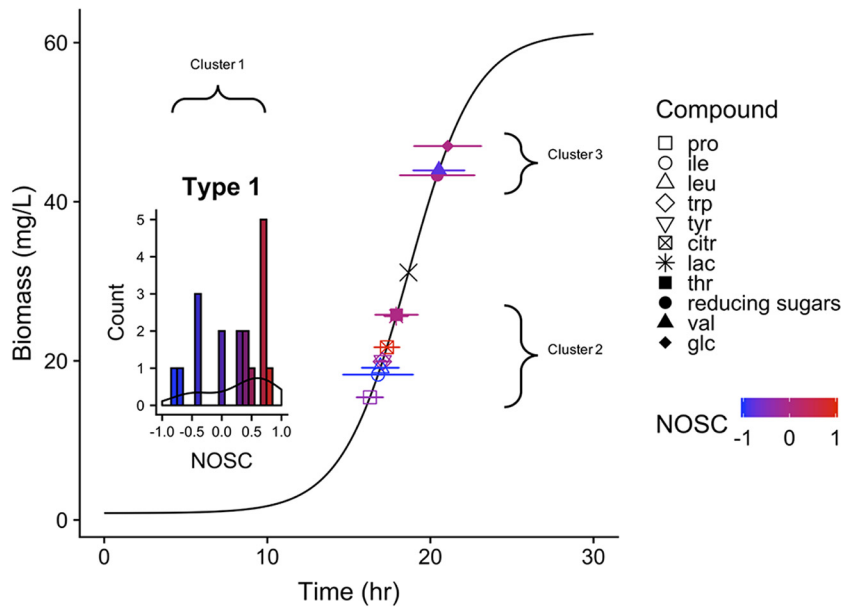
FIG 4 Usage window plot of *Paraburkholderia* sp. 1N growth on SESOM. Modeled depletion patterns of targeted carbon substrates are overlaid on the growth curve. Only substrates for which sufficient data allowed the fitting of a sigmoidal curve are depicted in the plot (type 2). The points represent the inflection point of depletion (t_{50}), and the horizontal bars represent the 90% usage window (modification of the fit window, w). The inflection point of the growth curve is also overlaid on the figure ($\times$). Many substrates were depleted substantially before the first sampling point (type 1 [Fig. S3]), and therefore, no kinetic data are available. A histogram of the targeted type 1 substrates is shown in the early portion of the growth curve for this reason. All depicted substrates are colored by their oxidation state (NOSC) and listed in order of increasing t_{50} in the key. Lactate is mostly obscured by threonine, which has a slightly later t_{50}.

Relationships between substrate depletion and hypothesized predictor variables (NOSC, specific μ_{max}, and concentration). We did not find NOSC or the sole C source growth rates, specific μ_{max}, to be reliable predictors of preferential substrate depletion, t_{50} (Fig. 6). The inclusion of untargeted, putatively characterized NOSC values (Fig. 6A) did not help build any relationship between the two variables. Specific μ_{max} was determined by growing *Paraburkholderia* sp. 1N on each substrate individually to determine maximal potential growth. While there was an upward trend between maximal growth rate (specific μ_{max}) and t_{50}, it is clear that inclusion of any of the type 1 substrates would invalidate that relationship (Fig. 6B). Similarly, there appears to have been an upward trend between initial compound concentration and substrate depletion preferences (t_{50} [Fig. 7A]), yet inclusion of three of the type 1 substrates, acetate, alanine, and glutamate, is not possible in such a relationship. Compounds at higher initial concentrations appear to have been used at higher rates (Fig. 7B) and for a longer window (Fig. 7C). Inclusion of type 1 substrates could maintain a nonlinear relationship, yet at this time only two points, glucose and valine, were driving the trend. More data from earlier in the growth curve would be necessary to confirm these relationships.

DISCUSSION

Three broad clusters of substrate depletion could be outlined during growth (Fig. 3). Many substrates belonging to the first cluster were depleted to their maximum potential before subsequent depletion of the second cluster began (Table 2 and Fig. S4). Distinct clustering of time-dependent substrate depletion implies multiauxic growth behavior of *Paraburkholderia* sp. 1N on SESOM. Within each phase of substrate use, there was coutilization of multiple substrates, which is similar to observations for other fast-growing *Bacillus* and *Pseudomonas* species (17, 31). The coexistence of sequential (multiauxic) and simultaneous (coutilization) substrate use as a metabolic strategy is more common than previously thought from investigation of the growth of
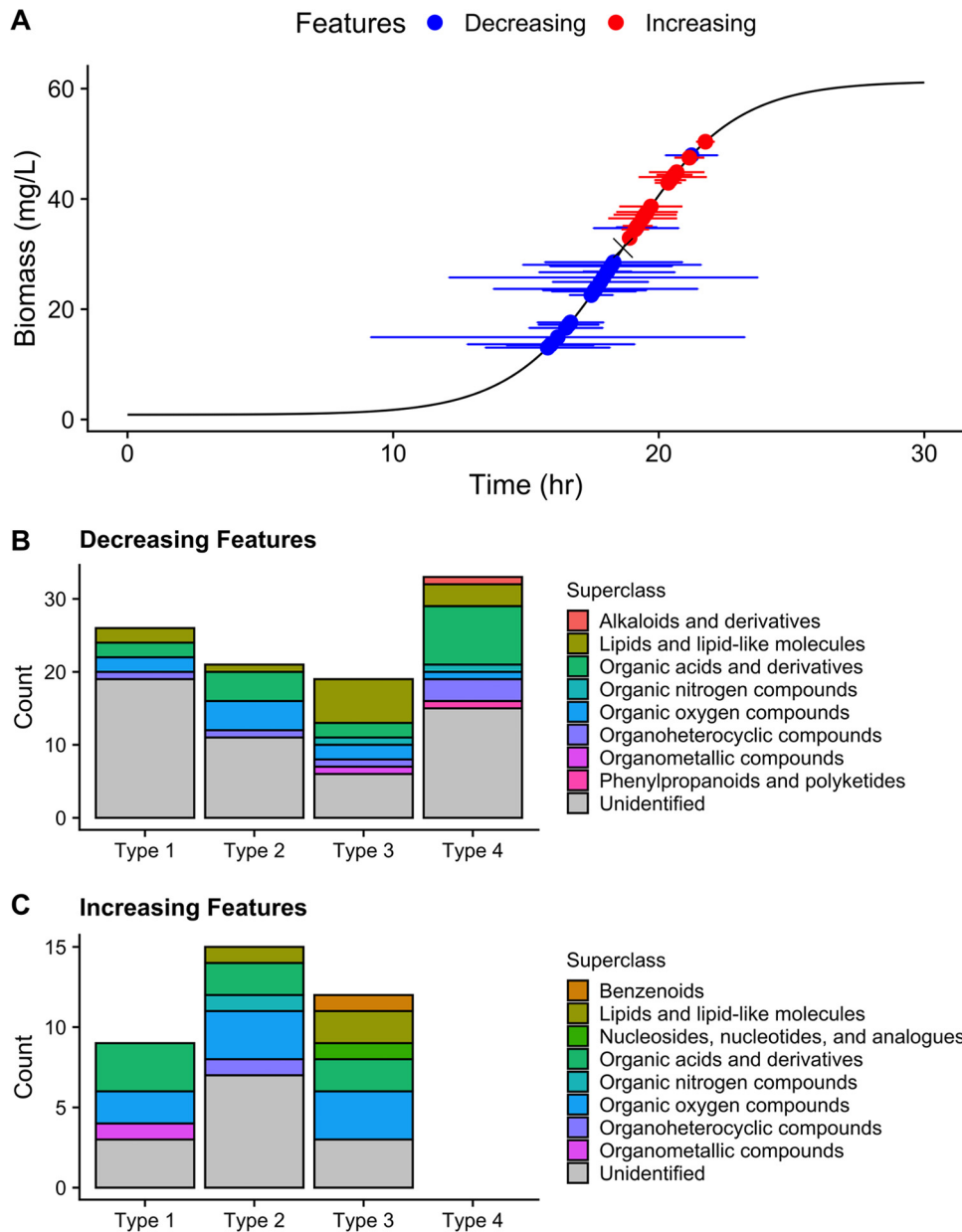
FIG 5 Untargeted features detected split by directionality of change. Type 2 features whose depletion or appearance could be modeled using a sigmoidal fit are depicted in a usage window plot (A). Points are overlaid over the growth curve at the inflection point of their depletion or appearance (t_{50}), while the horizontal bars represent the 90% usage window (modification of the fit window, width) of the feature. Decreasing and increasing features were sorted based on the kinetics and shape of their curve and sorted by superclass (B and C; type 1, early depletion or appearance/insufficient data for fit; type 2, sigmoidal curve fit; type 3, nonsigmoidal depletion or appearance; type 4, late depletion or appearance/insufficient data for fit).

heterotrophs in diverse, low-concentration media (48, 49). We observed that acetate, alanine, and glutamate likely provided the majority of carbon from SESOM for *Paraburkholderia* sp. 1N's biomass production in the first phase, lactate in the second, and reducing sugars coupled with valine in the final phase (Table 2 and Fig. 6). Inclusion of untargeted data indicates that there may have been many more compounds being used over longer periods within this multiphasic substrate removal pattern (Fig. 4A). Unfortunately, the inability to quantify putatively identified compounds leaves their potential contribution to biomass production unknown for this experiment.

In complex media, such as SESOM, translation and expression of all transporter
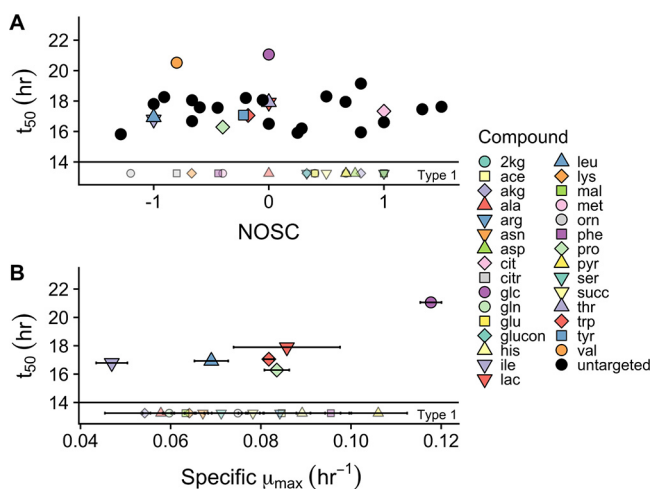
FIG 6 Model fit t_{50} values for substrates as a function of hypothesized predictor variables. (A) The midpoint of depletion, t_{50}, as a function of substrate nominal oxidation state of carbon. (B) t_{50} as a function of the specific growth rate (μ_{max}) of *Paraburkholderia* sp. 1N growing on that substrate as the sole C source. Error bars represent standard errors ($n = 3$). Both panels share the same key, though untargeted features are displayed only in Panel A. For both panels, type 1 substrates are depicted below the horizontal line and grayed out, as they have an x axis value (NOSC, specific μ_{max}) but could not be fit to a 4-point sigmoidal depletion curve.

systems and metabolic pathways present too high a cost (50), requiring a complex regulatory network to shift uptake dynamics. The observed clustering of substrate depletion is indicative of a metabolic network shift, though higher-resolution growth measurements are needed to determine whether *Paraburkholderia* sp. 1N is able to make these types of metabolic shifts with or without a slowdown in growth rate (51, 52). *Paraburkholderia* sp. 1N has a putative phosphoenolpyruvate protein of the phosphotransferase system (PTS), which is implicated in carbon catabolite repression in *Escherichia coli* as well as *Bacillus subtilis* and the selective use of sugars (33). Though a PTS system is present, there was no significant difference in the mean uptake of reducing sugars and glucose to suggest carbon catabolite repression. *Paraburkholderia* sp. 1N also has the Liv (leucine-isoleucine-valine) system, which is an ATP-binding cassette (ABC) transporter found in *E. coli* (53). It may be possible that *Paraburkholderia* sp. 1N can up- and downregulate one of the six annotated, amino acid-binding proteins (TC 3.A.1.4.1). These have been shown to be paralogues in other organisms and differ in amino acid specificity and affinity (53). Up- and downregulation of transporters with different affinities could explain the observed clustering of amino acid uptake patterns. Alternatively, similar ABC transporter systems have been found to have broad specificity (54), so another possibility is that the uptake of amino acids may not be under strict control at all. The predominance of increasing features in the exometabolome after the inflection point of growth (Fig. 5A), at timing similar to that of the switch to multiple sugar and valine metabolism, is indicative of a regulated metabolic shift. This may be due to changing nutrient availability or other stress encountered during batch growth and a resulting release of metabolites (55).

Paraburkholderia sp. 1N exhibits a growth strategy that falls outside traditional paradigms. While this isolate did show metabolic diversity that is in accordance with that of other fast-growing soil bacteria, it did not selectively use those substrates (glucose, histidine, phenylalanine, pyruvate, and lactate) that connote optimal growth rates (Fig. 7B). Coutilization of carbon sources is expected to boost microbial growth rate (33, 56), though at the expense of individual substrate uptake rates (57). While it is possible that clustered substrate usage may offer the advantage of an increased growth rate in a way not observed in individual specific μ_{max} estimates (Fig. 5B), this seems unlikely, as substantially lower biomass normalized depletion rates (millimoles per hour per gram of cells [dry weight]) were observed earlier during growth (Fig. 6B).
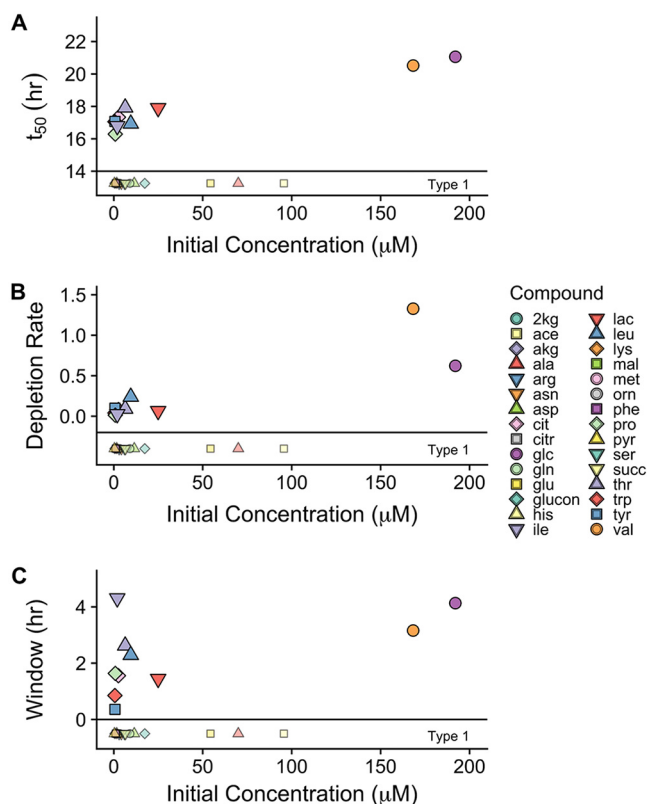
FIG 7 Model fit t_{50} values for substrates (A), depletion rate (B), and usage window (C) as a function of initial concentration. Depletion rate is depicted normalized to biomass (millimoles per hour per gram of cells [dry weight]). The window depicted (Panel C) is the estimated 90% usage window. Type 1 substrates are depicted below the horizontal line and grayed, as they have *x* axis value (initial concentration) but could not be fit to a 4-point sigmoidal depletion curve.

The lower depletion rates of earlier type 2 substrates may indicate a strategy of maximizing growth efficiency using these lower-concentration substrates even though they do not support higher growth rates. Either *Paraburkholderia* sp. 1N does not group with other copiotrophs or not all copiotrophs maximize growth rate at the expense of efficiency (10). Other observations of the coexistence of multiauxic and simultaneous substrate use tend to reinforce the idea that substrate selection is still based on affording the highest growth rate possible (31, 49). *Bacillus cereus* is one other example of a fast-growing, *r*-selected organism that has been observed to selectively take up substrates based on a mechanism outside maximizing growth rate (31).

Our results did not show that *Paraburkholderia* sp. 1N had any predilection for depleting more oxidized substrates first, contrary to observations from whole-soil communities (24). There was a slightly higher number of oxidized type 1 substrates (Fig. 3, inset), yet overall, there was no relationship between these parameters (Fig. 5). The form of regulation that best fits our observations is the multiauxic usage of substrate groups representing a mix of divergent oxidized and reduced compounds. This use of a more oxidized compound for energy generation, resulting in increased growth yield, has been frequently observed in simple, two-substrate mixtures (12). Increasingly, the coutilization of substrates is thought to be the result of optimal enzyme allocation (58), suggesting an advantage to the simultaneous use of glycolytic and gluconeogenic substrates (59, 60). Indeed, recent ^{13}C labeling experiments with a marine heterotroph have shown the "different and complementary roles" of simultaneously used amino acids (49). There is some evidence for this in the second grouping of substrates in which growth on citrate (NOSC = 1.00) was coupled with isoleucine and leucine (NOSC = −1.00), among others. This pattern of C utilization was observed in our data because

of our comprehensive tracking of multiple metabolites through time and grouping by metabolite use stage. This phenomenon may be missed if the reduced compound in the coupled pair or group is not also tracked, which is a possibility in many whole-soil data sets probing a small subset of isotopically labeled substrates (20, 22, 24).

The efficiency of biomass production of *Paraburkholderia* sp. 1N (CUE) was observed to be within reported ranges of *in situ* soil communities and soil isolates. The estimated CUE of 0.43 is well within those reported for other bacterial pure cultures (CUE_P, 0.2 to 0.8) as well as those reported for *in situ* soil communities (CUE_E, 0 to 0.85) (28, 61). This value is close to those reported for chemostat cultures of *Klebsiella aerogenes* NCTC 418 ($\sim$0.4) growing on limited glycerol concentrations in the $<20\,\mu M$ range, similar to many of the substrate concentration ranges in this medium (10). *Paraburkholderia* sp. 1N's cumulative CUE also aligns well with the proposed relationship between maximal growth rate and carbon use efficiency and puts its CUE alongside that of a considered oligotroph, *Rhodospirillaceae* sp. PX3.14 ($\mu_{max} = 0.126$ to 0.144; CUE $\sim$ 0.38) (62, 63). As mentioned previously, this high CUE and slow maximal growth rate, compared to those of other bacteria, may indicate that *Paraburkholderia* sp. 1N is on the boundary between the copiotrophic and oligotrophic ecological distinctions (62). Interestingly, predictions of CUE based on genome size alone show that *Paraburkholderia* sp. 1N's estimated CUE of 0.43 is around the potential CUE of 0.4 predicted for its genome size of 11.1 Mb (64). Thus, while this organism may require greater maintenance resource allocation than others with smaller genomes, it is able to grow at an efficiency near its predicted potential in a highly diverse and carbon-limiting medium.

Predicting the use efficiency of individual substrates (65), based on temporal alignment between uptake and overall CUE, is a tempting next step but one that has many potential pitfalls. For instance, the second cluster of substrate utilization (Fig. 4) temporally aligns with the highest estimate of instantaneous CUE (Fig. 3). It might be reasonable to infer that this cluster of amino acids and organic acids is used most efficiently during this time of high biomass production, yet there is a possibility for a disconnect between assimilation and actual metabolic use. The population may employ a strategy of transforming the molecule to protect it from potential use by other microorganisms or for intracellular storage (66). The simultaneous assimilation of multiple substrates in distinct groups, which we observed (Fig. 3), could result in the microbial population preferentially routing one substrate to dissimilatory pathways and the other to assimilation (59). This would result in substrates with disparate individual use efficiencies that produce the observed average CUE.

Substrate concentration differences were up to 2 orders of magnitude in some cases for the SESOM used in this experiment (Table 2) and may have overwhelmed any influence of substrate energy content (NOSC) on utilization preference. Studies with equimolar initial substrate concentrations are needed for quantitation and identification of substrate uptake preferences. The application of isotopic substrate labeling in such studies could further probe hypothetical relationships between substrate groups and individual substrate use efficiencies. Understanding the effects of both compound identity and compound concentration is instrumental to the implementation of substrate uptake framework in environmental prediction models.

Paraburkholderia sp. 1N belongs to a clade of bacteria abundant in forest soils which broadly influence C cycling via phenolic acid-induced priming (46). We have shown that *Paraburkholderia* sp. 1N preferentially uses LMW substrates in SESOM in three distinct phases (Fig. 5). Lower-concentration amino acids and organic acids were used earlier on in the growth curve, followed by higher-concentration sugars and an amino acid coupled with NH_4^+ uptake (Fig. 5 and Fig. S5). Moving forward, time-resolved exo-metabolomic footprinting studies of key species in soil microbial communities of interest could aid our understanding of net observations of LMW cycling and the underlying mechanisms. To evaluate the physiological profile exhibited by *Paraburkholderia* sp. 1N as representative of other *r*-selected populations, further investigations of other species are needed, based on community dominance or ranging in phylogenetic or physiological differences.

MATERIALS AND METHODS

Preparation of SESOM as an undefined medium for isolation and growth. Soil was collected under a hemlock-dominated stand in Arnot Forest near previous experimental plots (67, 68). Field-moist soil samples were immediately placed in a cooler and stored at 4°C until further processing (<24 h). Soil-extracted, solubilized organic matter (SESOM) was prepared using a modified water extraction procedure (47). Briefly, 40 g of air-dried Oa horizon from Arnot Forest was mixed with 200 ml of 18.2 MΩ-cm water in 250-ml Nalgene bottles and shaken on an end-to-end shaker for 1 h at room temperature. Bottles were then left to stand for 24 h and then sequentially filtered through 1.6-μm glass microfiber (GF/A), 0.45-μm polyethersulfone (PES), and then 0.2-μm PES filters to produce a filter-sterilized solution. Multiple bottles were extracted at once and combined to provide sufficient SESOM for experimental purposes. The extracted solution was diluted 2-fold for all growth experiments to produce concentrations that might be more realistically encountered in percolating pore water following a rainfall event.

Isolation. *Paraburkholderia* sp. 1N was isolated from field-moist B horizon found at the site. Briefly, agar plates (15 g/liter) were made with SESOM as the sole C source (10× dilution). For isolate enrichment, fresh soil was shaken with deionized (DI) water (1:10 ratio) for 1 h and then let sit for 24 h at room temperature. Serial dilutions were created using Winogradsky salts (69) and 100 μl was spread onto plates. Plates were incubated at room temperature in the dark for 3 to 14 days, and colonies were chosen at first appearance and restreaked on fresh SESOM 10×-dilution plates. Three separate plating rounds were conducted. Cellular morphology was determined microscopically, and growth was checked in liquid SESOM (2× dilution). *Paraburkholderia* sp. 1N has circular entire-colony morphology and is rod shaped. The isolate was stored on SESOM agar plates at 4°C, and single colonies were used to initiate a starter flask before each experiment of interest.

DNA extraction, genomic analysis, and phylogenetic analysis. Genomic DNA was extracted from pelleted cells from a liquid culture of the isolate on 10 ml of SESOM (2× dilution) (70) and submitted to the Cornell University Sequencing Facility for sequencing using three multiplexed runs of Illumina MiSeq Nano (2 × 250 bp). Raw sequencing data were quality preprocessed with Trimmomatic (v.0.32) (71) and FastX Toolkit (v.0.7) (72) and then assembled with SPAdes (v.3.10.1) (73). Open reading frames were predicted using Prodigal (v.2.6.2) (74). The assembly was then uploaded to the KBase web server (75) for further processing. A phylogenetic tree was constructed using the KBase application Insert Set of Genomes Into Species Tree (v.2.1.10), dependent on Fast-Tree2 (76) to provide context within 50 neighboring genomes. Genomic annotation was then conducted using the KBase application Annotate Microbial Assembly, which utilizes the RAST toolkit (77).

Growth on SESOM. Acid-washed and autoclaved 125-ml Erlenmeyer flasks were used for all growth curve experiments. A starter flask containing 50 ml of SESOM was inoculated with a single colony of *Paraburkholderia* sp. 1N and grown overnight on a shaker at 150 rpm until reaching log phase. A 0.5-ml subsample (optical density at 600 nm [OD_{600}] = 0.0658, or ~7.64 mg/liter of biomass) was used to inoculate each experimental flask for the growth curve assessment (starting biomass = 0.0757 mg/liter). Assessment of the growth curve was conducted using OD_{600}. A growth curve was then fit using a 4-point sigmoidal function (Fig. 1).

To allow the tracking of substrate depletion during growth, three flasks were destructively harvested at four points along the growth curve (17, 19, 22, and 24 h). Points were chosen to cover the breadth of the exponential phase of growth and the beginning of stationary phase. While each flask was independent, they were treated as replicates for each time point in subsequent analyses. During each destructive-sampling event, 10 ml was removed for analyses on unfiltered components (TOC, TN, and cellular protein content) while the remaining 40 ml was filtered through 0.2-μm PES filters to remove cellular biomass and stored frozen in separate aliquots for further analyses (pH, TOC, TN, reducing sugars, NO_3^-, NO_2^-, NH_4^+, ninhydrin-N, ^1H NMR, and LC-HRMS). Since all media were from a single extraction event and of limited volume, all initial medium values were analyzed only once for each analyte of interest. A Shimadzu TOC-V$_{CPN}$ was used to measure nonpurgeable organic carbon (referred to as total organic carbon) and total nitrogen using a 2% acidification (0.2 M HCl) and 1.5 min sparge time using high-temperature (720°C) catalytic (Pt) oxidation. Cellular protein content was measured on dual analytical replicates using a modified Bradford protein assay using bovine serum albumin (BSA) as the standard (78). Reducing sugars were measured using a colorimetric alkaline ferricyanide reaction (79). The colorimetric Griess reaction method was used to measure NO_3^- and NO_2^- (80, 81). A modified Berthelot reaction was used to measure NH_4^+ (82). Total free amino acids were estimated using a ninhydrin method (referred to as ninhydrin-N) (83–85). All colorimetric samples were analyzed using a Shimadzu UV-2600 UV-visible (UV-Vis) spectrophotometer.

Estimation of carbon use efficiency determined via cell filtration. Estimates of cumulative CUE (milligrams of C in biomass per milligrams of C assimilated) could be derived from measurements of initial SESOM in comparison to sampled time points before and after cell removal via 0.2-μm filtration (PES),

$$CUE = \frac{(\text{unfiltered solution C})_t - (0.2\text{-μm-filtered solution C})_t}{(\text{unfiltered solution C})_{t-1} - (\text{unfiltered solution C})_t} \quad (1)$$

where all values are in milligrams of C per liter. Carbon measurements were made using a Shimadzu TOC-V$_{CPN}$ as described above. Due to the large size of the injection needle port, measurements of unfiltered solution contained microbial cells and resulting values represent cellular as well as extracellular carbon in solution.

Time-resolved exometabolomic footprinting. (i) Targeted metabolites via ^{1}H NMR. Samples were analyzed by ^{1}H NMR using modified methods previously reported for extracted soil solutions (47, 86). Briefly 30 ml of filtered SESOM medium was immediately frozen and lyophilized. Samples were then reconstituted with 300 μl of 18.2 MΩ-cm water. After vortexing, samples were buffered to pH 7.0 with an addition of 200 μl of sodium hydrogen phosphate (0.1 mM, pH 7.0) made with 25% D_2O (vol/vol) to provide a lock signal and containing 1 mM sodium 3-trimethylsilyl-[2,2,3,3,-D_4]-1-propionic acid (TMSP). Solutions were transferred to 5-mm NMR glass tubes (length, 7 in.; Wilmad "Economy"). Spectral referencing was conducted in reference to the TMSP (final concentration = 0.4 mM). All NMR spectra were collected at 500 MHz at room temperature on a Bruker AV 500 operated by Bruker TopSpin 3.5.7 using a 10% D_2O and water peak suppression program (one-dimensional [1D] nuclear Overhauser effect spectroscopy [NOESY] with presaturation and spoil gradients [noesygppr1d]) with 32 scans/sample and a 5-s relaxation delay for a total of 256 transients. Within MestReNova (v.12.0.0-20080), spectra were Fourier transformed and zero-filled to 64,000 data points. Spectra were then linearly phase shifted and apodized using a 0-Hz exponential function. All spectra were manually phase corrected (PH0, −26; PH1, 6) and baseline corrected using the built-in polynomial fit function. All spectra were reference shifted so TMSP was 0.00 ppm. Lastly, residual water peak was removed using the signal suppression tool with selectivity at 24 centered on the 4.7-ppm signal. Compound identification was initiated by matching peaks of interest with suitable references (47, 87) as well as using online spectral data banks (Human Metabolome Database) to confirm multiplicity and chemical shift. Once identified, integrating regions were defined and used for integration on all samples (Table S2).

(ii) Targeted metabolites via LC-HRMS. Another set of filtered subsamples were immediately frozen at −20°C. These samples were thawed and analyzed using LC-HRMS. Samples were run on a Thermo Scientific Dionex Ultimate 3000 liquid chromatography system coupled to a Q Exactive orbitrap mass spectrometer. Two separate methods were employed: a reversed-phased approach using a Acquity ultraperformance liquid chromatography (UPLC) Waters C_{18} column (2.1 by 100 mm by 1.7 μm) as the stationary phase and negative electrospray ionization to identify metabolites (88, 89) (Table 2, LC-HRMS-Metabo method) as well as a hydrophilic interaction approach using a Waters XBridge column (4.6 by 100 mm by 3.5 μm) and electrospray ionization with polarity switching for amino acids (90) (Table 2, LC-HRMS-AA method). Quality control (QC) checks were run every 10 samples with a 30% standard-deviation (SD) limit. All data were analyzed using an internally constructed template within the Thermo Scientific Xcalibur 3.0 Quan browser. The template was built using standards of all identified compounds and run between 0 and 15 μM.

(iii) Untargeted metabolites via LC-HRMS. Data from the reversed-phase method were alternatively processed using an untargeted approach via XCMS online v.2.3.0 (91). Detailed processing parameters are included in the supplemental material. XCMS online output with CAMERA annotation was then imported and further processed using R 3.6.0 (92). Features of interest were further refined based on the following selection criteria: |ln(fold change)| > 1, $P < 0.05$, and maxint >10^7). Metabolites already targeted were removed based on overlapping m/z (±0.001) and retention time (±30 s). The refined CAMERA output was then used as input for MetaboQuest (http://omicscraft.com/MetaboQuest/), where m/z was searched against several databases (PubChem, HMDB, LIPID MAPS, KEGG, MMCD, and METLIN) and the lowest error (parts per million) hit was chosen for putative identification (level 2) (93). Those returned results containing InChIKeys were then classified using ClassyFire (https://cfb.fiehnlab.ucdavis.edu/) (94). The superclass level, which includes 26 organic and 5 inorganic categories, was chosen as the most informative way to present compound differences as determined by this untargeted approach.

Curve fits for substrate depletion. Substrate depletion was modeled using R 3.6.0 (92). Data were fit using the nls.multstart package (95) to fit sigmoidal uptake curves as described previously (17, 31). Briefly, a nonlinear modeling approach allows the fitting of a 4-point curve using the following equation:

$$y = \frac{a}{1 + e^{\frac{x - t_{50}}{w}}} + o \qquad (2)$$

The resulting four parameters produced by the fit relate to the amplitude of the curve (*a*), the midpoint of compound depletion from the medium (t_{50}), the width of the concentration decrease (*w*), and the offset or predicted final value (*o*). The width (*w*) is mathematically defined as the time it takes for the exponent of *e* to go from 1 to −1. This parameter has been modified to depict the time from 10% of substrate utilization [(*a* − *o*) × 0.9] to 90% of substrate utilization [(*a* − *o*) × 0.1] and is depicted in later figures as a 90% usage window. For appearance curves, the signs are changed for a portion of the equation, [−(*x* − t_{50})], to invert the model fit. More generally, decreasing and increasing concentrations of compounds in the media were grouped into four different categories: type 1, early depletion or appearance and insufficient data for curve fitting; type 2, sigmoidal fit; type 3, sufficient data but nonsigmoidal shape; and type 4, late depletion or appearance and insufficient data for curve fitting (Fig. S4 to S12).

Curves were visually inspected to ensure that measured data were sufficient and appropriate to fit using this nonlinear function. In some cases, depletion occurred predominantly before or after the sampling interval (types 1 and 4). In these cases, nonlinear depletion curves were not fit since no data were available to indicate a suitable t_{50} or the steepness of the curve around this inflection point. Parameters of interest (t_{50}) and (width) were extracted and used to construct usage window plots to aid in the visualization of substrate depletion preferences and overlapping usage windows. A modified version of the width parameter, 90% usage window, was created by solving the fitted curve for the time of 10% of usage [(amplitude − offset) × 0.9] as well 90% of substrate utilization [(amplitude − offset) × 0.1]. Following the protocol outlined in the work of Erbilgin et al., the differential of the 4-point

sigmoidal fit was used to solve for the slope of all substrate depletion curves (31). The maximum rate was then extracted within the time frame of the experiment (0 to 24 h).

Determination of substrate specific growth rates of *Paraburkholderia* sp. 1N on targeted substrates. Specific μ_{max} was determined by culturing on each targeted substrate as the sole carbon source. The medium used for these trials consisted of $1\times$ Wolfe's vitamin supplement (ATCC MD-VS), $1\times$ Wolfe's trace mineral solution (ATCC MD-TMS), ammonium chloride (1.5 g/liter), potassium phosphate (0.5 g/liter), and each substrate supplied at an equivalent C content (200 mg of C/liter). *Paraburkholderia* sp. 1N was grown overnight in 10 ml of each sole C medium and then 100 μl was removed into a sterile 2-ml centrifuge tube. Biomass was pelleted at 5,000 $\times$ *g* and washed 3 times using fresh medium. The sample was then vortexed, 200-μl subsamples were placed into a 96-well plate, and growth was monitored hourly using a microplate reader at 595 nm (FilterMax F5; Molecular Devices). A total of 3 replicates and an uninoculated blank were used for each sole C medium. Data were imported into R 3.6.0 (92), and the growth rate package (96) was used to fit growth curves for each replicate and extract the average maximum μ_{max}.

Data availability. The genome assembly for *Paraburkholderia* sp. 1N can be accessed via the NCBI portal using the BioProject accession number PRJNA590275. Draft genome annotation, along with associated material, can be found in KBase (https://narrative.kbase.us/narrative/55022). All LC-HRMS and ^{1}H NMR raw data files, associated metadata, as well as processed output have been deposited to the EMBL-EBI MetaboLights database with the identifier MTBLS1692 (https://www.ebi.ac.uk/metabolights/MTBLS1692) (97).

SUPPLEMENTAL MATERIAL

Supplemental material is available online only.

SUPPLEMENTAL FILE 1, PDF file, 7.3 MB.

REFERENCES

1. Roth V-N, Lange M, Simon C, Hertkorn N, Bucher S, Goodall T, Griffiths RI, Mellado-Vázquez PG, Mommer L, Oram NJ, Weigelt A, Dittmar T, Gleixner G. 2019. Persistence of dissolved organic matter explained by molecular changes during its passage through soil. Nat Geosci 12:755–761. https://doi.org/10.1038/s41561-019-0417-4.

2. Ellert B, Gregorich E, McFee W, Kelly J. 1995. Management-induced changes in the actively cycling fractions of soil organic matter, p 119–138. *In* McFee WW, Kelly M (ed), Carbon forms and functions in forest soils. American Society of Agronomy, Crop Science Society of America, and Soil Science Society of America Inc, Madison, WI. https://doi.org/10.2136/1995.carbonforms.c7.

3. Hill PW, Farrar JF, Jones DL. 2008. Decoupling of microbial glucose uptake and mineralization in soil. Soil Biol Biochem 40:616–624. https://doi.org/10.1016/j.soilbio.2007.09.008.

4. van Hees PA, Johansson E, Jones D. 2008. Dynamics of simple carbon compounds in two forest soils as revealed by soil solution concentrations and biodegradation kinetics. Plant Soil 310:11–23. https://doi.org/10.1007/s11104-008-9623-3.

5. van Hees PAW, Jones DL, Finlay R, Godbold DL, Lundström US. 2005. The carbon we do not see—the impact of low molecular weight compounds on carbon dynamics and respiration in forest soils: a review. Soil Biol Biochem 37:1–13. https://doi.org/10.1016/j.soilbio.2004.06.010.

6. Glanville H, Hill P, Schnepf A, Oburger E, Jones D. 2016. Combined use of empirical data and mathematical modelling to better estimate the microbial turnover of isotopically labelled carbon substrates in soil. Soil Biol Biochem 94:154–168. https://doi.org/10.1016/j.soilbio.2015.11.016.

7. Glanville H, Rousk J, Golyshin P, Jones D. 2012. Mineralization of low molecular weight carbon substrates in soil solution under laboratory and field conditions. Soil Biol Biochem 48:88–95. https://doi.org/10.1016/j.soilbio.2012.01.015.

8. Jones D, Dennis P, Owen A, Van Hees P. 2003. Organic acid behavior in soils—misconceptions and knowledge gaps. Plant Soil 248:31–41. https://doi.org/10.1023/A:1022304332313.

9. Tang JY, Riley WJ. 2013. A total quasi-steady-state formulation of substrate uptake kinetics in complex networks and an example application to microbial litter decomposition. Biogeosciences 10:8329–8351. https://doi.org/10.5194/bg-10-8329-2013.

10. Roller BRK, Schmidt TM. 2015. The physiology and ecological implications of efficient growth. ISME J 9:1481–1487. https://doi.org/10.1038/ismej.2014.235.

11. Creamer CA, Jones DL, Baldock JA, Farrell M. 2014. Stoichiometric controls upon low molecular weight carbon decomposition. Soil Biol Biochem 79:50–56. https://doi.org/10.1016/j.soilbio.2014.08.019.

12. Gommers PJ, van Schie BJ, van Dijken JP, Kuenen JG. 1988. Biochemical limits to microbial-growth yields—an analysis of mixed substrate utilization. Biotechnol Bioeng 32:86–94. https://doi.org/10.1002/bit.260320112.

13. Maharjan RP, Ferenci T. 2005. Metabolomic diversity in the species Escherichia coli and its relationship to genetic population structure. Metabolomics 1:235–242. https://doi.org/10.1007/s11306-005-0002-2.

14. MacKenzie DA, Defernez M, Dunn WB, Brown M, Fuller LJ, de Herrera SRMS, Günther A, James SA, Eagles J, Philo M, Goodacre R, Roberts IN. 2008. Relatedness of medically important strains of Saccharomyces cerevisiae as revealed by phylogenetics and metabolomics. Yeast 25:501–512. https://doi.org/10.1002/yea.1601.

15. Pope GA, MacKenzie DA, Defernez M, Aroso MAMM, Fuller LJ, Mellon FA, Dunn WB, Brown M, Goodacre R, Kell DB, Marvin ME, Louis EJ, Roberts IN. 2007. Metabolic footprinting as a tool for discriminating between brewing yeasts. Yeast 24:667–679. https://doi.org/10.1002/yea.1499.

16. Behrends V, Geier B, Williams HD, Bundy JG. 2013. Direct assessment of metabolite utilization by Pseudomonas aeruginosa during growth on artificial sputum medium. Appl Environ Microbiol 79:2467–2470. https://doi.org/10.1128/AEM.03609-12.

17. Behrends V, Ebbels TMD, Williams HD, Bundy JG. 2009. Time-resolved metabolic footprinting for nonlinear modeling of bacterial substrate utilization. Appl Environ Microbiol 75:2453–2463. https://doi.org/10.1128/AEM.01742-08.

18. Morrissey EM, Mau RL, Hayer M, Liu X-JA, Schwartz E, Dijkstra P, Koch BJ, Allen K, Blazewicz SJ, Hofmockel K, Pett-Ridge J, Hungate BA. 2019. Evolutionary history constrains microbial traits across environmental variation. Nat Ecol Evol 3:1064–1069. https://doi.org/10.1038/s41559-019-0918-y.

19. Fierer N, Bradford MA, Jackson RB. 2007. Toward an ecological classification of soil bacteria. Ecology 88:1354–1364. https://doi.org/10.1890/05-1839.

20. Bradford MA, Keiser AD, Davies CA, Mersmann CA, Strickland MS. 2013. Empirical evidence that soil carbon formation from plant inputs is positively related to microbial growth. Biogeochemistry 113:271–281. https://doi.org/10.1007/s10533-012-9822-0.

21. Brant JB, Sulzman EW, Myrold DD. 2006. Microbial community utilization of added carbon substrates in response to long-term carbon input manipulation. Soil Biol Biochem 38:2219–2232. https://doi.org/10.1016/j.soilbio.2006.01.022.

22. Gunina A, Dippold MA, Glaser B, Kuzyakov Y. 2014. Fate of low molecular weight organic substances in an arable soil: from microbial uptake to utilisation and stabilisation. Soil Biol Biochem 77:304–313. https://doi.org/10.1016/j.soilbio.2014.06.029.

23. Frey SD, Lee J, Melillo JM, Six J. 2013. The temperature response of soil microbial efficiency and its feedback to climate. Nat Clim Chang 3:395–398. https://doi.org/10.1038/nclimate1796.

24. Gunina A, Smith AR, Kuzyakov Y, Jones DL. 2017. Microbial uptake and utilization of low molecular weight organic substrates in soil depend on carbon oxidation state. Biogeochemistry 133:89–100. https://doi.org/10.1007/s10533-017-0313-1.

25. Sugai SF, Schimel JP. 1993. Decomposition and biomass incorporation of 14c-labeled glucose and phenolics in taiga forest floor: effect of substrate quality, successional state, and season. Soil Biol Biochem 25:1379–1389. https://doi.org/10.1016/0038-0717(93)90052-D.

26. LaRowe DE, Van Cappellen P. 2011. Degradation of natural organic matter: a thermodynamic analysis. Geochim Cosmochim Acta 75:2030–2042. https://doi.org/10.1016/j.gca.2011.01.020.

27. Roels J. 1980. Application of macroscopic principles to microbial metabolism. Biotechnol Bioeng 22:2457–2514. https://doi.org/10.1002/bit.260221202.

28. Manzoni S, Taylor P, Richter A, Porporato A, Agren GI. 2012. Environmental and stoichiometric controls on microbial carbon-use efficiency in soils. New Phytol 196:79–91. https://doi.org/10.1111/j.1469-8137.2012.04225.x.

29. Kleber M. 2010. What is recalcitrant soil organic matter? Environ Chem 7:320–332. https://doi.org/10.1071/EN10006.

30. Linton JD, Stephenson RJ. 1978. A preliminary study on growth yields in relation to the carbon and energy content of various organic growth substrates. FEMS Microbiol Lett 3:95–98. https://doi.org/10.1111/j.1574-6968.1978.tb01891.x.

31. Erbilgin O, Bowen BP, Kosina SM, Jenkins S, Lau RK, Northen TR. 2017. Dynamic substrate preferences predict metabolic properties of a simple microbial consortium. BMC Bioinformatics 18:57. https://doi.org/10.1186/s12859-017-1478-2.

32. Kremling A, Geiselmann J, Ropers D, de Jong H. 2015. Understanding carbon catabolite repression in Escherichia coli using quantitative models. Trends Microbiol 23:99–109. https://doi.org/10.1016/j.tim.2014.11.002.

33. Görke B, Stülke J. 2008. Carbon catabolite repression in bacteria: many ways to make the most out of nutrients. Nat Rev Microbiol 6:613–624. https://doi.org/10.1038/nrmicro1932.

34. Kovárová-Kovar K, Egli T. 1998. Growth kinetics of suspended microbial cells: from single-substrate-controlled growth to mixed-substrate kinetics. Microbiol Mol Biol Rev 62:646–666. https://doi.org/10.1128/MMBR.62.3.646-666.1998.

35. Egli T. 1995. The ecological and physiological significance of the growth of heterotrophic microorganisms with mixtures of substrates. Adv Microb Ecol 14:305–386. https://doi.org/10.1007/978-1-4684-7724-5_8.

36. Egli T. 2015. Microbial growth and physiology: a call for better craftsmanship. Front Microbiol 6:287. https://doi.org/10.3389/fmicb.2015.00287.

37. Swenson TL, Jenkins S, Bowen BP, Northen TR. 2015. Untargeted soil metabolomics methods for analysis of extractable organic matter. Soil Biol Biochem 80:189–198. https://doi.org/10.1016/j.soilbio.2014.10.007.

38. Baran R, Brodie EL, Mayberry-Lewis J, Hummel E, Da Rocha UN, Chakraborty R, Bowen BP, Karaoz U, Cadillo-Quiroz H, Garcia-Pichel F, Northen TR. 2015. Exometabolite niche partitioning among sympatric soil bacteria. Nat Commun 6:8289. https://doi.org/10.1038/ncomms9289.

39. Sasse J, Kant J, Cole BJ, Klein AP, Arsova B, Schlaepfer P, Gao J, Lewald K, Zhalnina K, Kosina S, Bowen BP, Treen D, Vogel J, Visel A, Watt M, Dangl JL, Northen TR. 2019. Multilab EcoFAB study shows highly reproducible physiology and depletion of soil metabolites by a model grass. New Phytol 222:1149–1160. https://doi.org/10.1111/nph.15662.

40. Jenkins S, Swenson TL, Lau R, Rocha AM, Aaring A, Hazen TC, Chakraborty R, Northen TR. 2017. Construction of viable soil defined media using quantitative metabolomics analysis of soil metabolites. Front Microbiol 8:2618. https://doi.org/10.3389/fmicb.2017.02618.

41. Swenson TL, Karaoz U, Swenson JM, Bowen BP, Northen TR. 2018. Linking soil biology and chemistry in biological soil crust using isolate exometabolomics. Nat Commun 9:19. https://doi.org/10.1038/s41467-017-02356-9.

42. Wilhelm RC, Cyle KT, Martinez CE, Karasz DC, Newman JD, Buckley DH. 18 August 2020. Paraburkholderia solitsugae sp. nov. and Paraburkholderia elongata sp. nov., phenolic acid-degrading bacteria isolated from forest soil and emended description of Paraburkholderia madseniana. Int J Syst Evol Microbiol https://doi.org/10.1099/ijsem.0.004387.

43. Beukes CW, Palmer M, Manyaka P, Chan WY, Avontuur JR, van Zyl E, Huntemann M, Clum A, Pillay M, Palaniappan K, Varghese N, Mikhailova N, Stamatis D, Reddy TBK, Daum C, Shapiro N, Markowitz V, Ivanova N, Kyrpides N, Woyke T, Blom J, Whitman WB, Venter SN, Steenkamp ET. 2017. Genome data provides high support for generic boundaries in Burkholderia sensu lato. Front Microbiol 8:1154. https://doi.org/10.3389/fmicb.2017.01154.

44. Dobritsa AP, Samadpour M. 2016. Transfer of eleven species of the genus Burkholderia to the genus Paraburkholderia and proposal of Caballeronia gen. nov. to accommodate twelve species of the genera Burkholderia and Paraburkholderia. Int J Syst Evol Microbiol 66:2836–2846. https://doi.org/10.1099/ijsem.0.001065.

45. Sawana A, Adeolu M, Gupta RS. 2014. Molecular signatures and phylogenomic analysis of the genus Burkholderia: proposal for division of this genus into the emended genus Burkholderia containing pathogenic organisms and a new genus Paraburkholderia gen. nov. harboring environmental species. Front Genet 5:429. https://doi.org/10.3389/fgene.2014.00429.

46. Zwetsloot MJ, Ucros JM, Wickings K, Wilhelm RC, Sparks J, Buckley DH, Bauerle TL. 2020. Prevalent root-derived phenolics drive shifts in microbial community composition and prime decomposition in forest soil. Soil Biol Biochem 145:107797. https://doi.org/10.1016/j.soilbio.2020.107797.

47. Liebeke M, Brozel VS, Hecker M, Lalk M. 2009. Chemical characterization

of soil extract as growth media for the ecophysiological study of bacteria. Appl Microbiol Biotechnol 83:161–173. https://doi.org/10.1007/s00253-009-1965-0.

48. Fei F, diCenzo GC, Bowdish DME, McCarry BE, Finan TM. 2016. Effects of synthetic large-scale genome reduction on metabolism and metabolic preferences in a nutritionally complex environment. Metabolomics 12:23. https://doi.org/10.1007/s11306-015-0928-y.

49. Perrin E, Ghini V, Giovannini M, Di Patti F, Cardazzo B, Carraro L, Fagorzi C, Turano P, Fani R, Fondi M. 2020. Diauxie and co-utilization of carbon sources can coexist during bacterial growth in nutritionally complex environments. Nat Commun 11:3135. https://doi.org/10.1038/s41467-020-16872-8.

50. Dekel E, Alon U. 2005. Optimality and evolutionary tuning of the expression level of a protein. Nature 436:588–592. https://doi.org/10.1038/nature03842.

51. Chu D, Barnes DJ. 2016. The lag-phase during diauxic growth is a trade-off between fast adaptation and high growth rate. Sci Rep 6:25191. https://doi.org/10.1038/srep25191.

52. New AM, Cerulus B, Govers SK, Perez-Samper G, Zhu B, Boogmans S, Xavier JB, Verstrepen KJ. 2014. Different levels of catabolite repression optimize growth in stable and variable environments. PLoS Biol 12:e1001764. https://doi.org/10.1371/journal.pbio.1001764.

53. Hosie AHF, Poole PS. 2001. Bacterial ABC transporters of amino acids. Res Microbiol 152:259–270. https://doi.org/10.1016/S0923-2508(01)01197-4.

54. Hosie AHF, Allaway D, Galloway CS, Dunsby HA, Poole PS. 2002. *Rhizobium leguminosarum* has a second general amino acid permease with unusually broad substrate specificity and high similarity to branched-chain amino acid transporters (Bra/LIV) of the ABC family. J Bacteriol 184:4071–4080. https://doi.org/10.1128/jb.184.15.4071-4080.2002.

55. Novotna J, Vohradsky J, Berndt P, Gramajo H, Langen H, Li X-M, Minas W, Orsaria L, Roeder D, Thompson CJ. 2003. Proteomic studies of diauxic lag in the differentiating prokaryote Streptomyces coelicolor reveal a regulatory network of stress-induced proteins and central metabolic enzymes. Mol Microbiol 48:1289–1303. https://doi.org/10.1046/j.1365-2958.2003.03529.x.

56. Kleijn RJ, Buescher JM, Le Chat L, Jules M, Aymerich S, Sauer U. 2010. Metabolic fluxes during strong carbon catabolite repression by malate in Bacillus subtilis. J Biol Chem 285:1587–1596. https://doi.org/10.1074/jbc.M109.061747.

57. Hermsen R, Okano H, You C, Werner N, Hwa T. 2015. A growth-rate composition formula for the growth of E. coli on co-utilized carbon substrates. Mol Syst Biol 11:801. https://doi.org/10.15252/msb.20145537.

58. Wang X, Xia K, Yang X, Tang C. 2019. Growth strategy of microbes on mixed carbon sources. Nat Commun 10:1279. https://doi.org/10.1038/s41467-019-09261-3.

59. Kukurugya MA, Mendonca CM, Solhtalab M, Wilkes RA, Thannhauser TW, Aristilde L. 2019. Multi-omics analysis unravels a segregated metabolic flux network that tunes co-utilization of sugar and aromatic carbons in Pseudomonas putida. J Biol Chem 294:8464–8479. https://doi.org/10.1074/jbc.RA119.007885.

60. Okano H, Hermsen R, Kochanowski K, Hwa T. 2020. Regulation underlying hierarchical and simultaneous utilization of carbon substrates by flux sensors in Escherichia coli. Nat Microbiol 5:206–215. https://doi.org/10.1038/s41564-019-0610-7.

61. Geyer KM, Kyker-Snowman E, Grandy AS, Frey SD. 2016. Microbial carbon use efficiency: accounting for population, community, and ecosystem-scale controls over the fate of metabolized organic matter. Biogeochemistry 127:173–188. https://doi.org/10.1007/s10533-016-0191-y.

62. Roller BRK, Stoddard SF, Schmidt TM. 2016. Exploiting rRNA operon copy number to investigate bacterial reproductive strategies. Nat Microbiol 1:16160. https://doi.org/10.1038/nmicrobiol.2016.160.

63. Dethlefsen L, Schmidt TM. 2007. Performance of the translational apparatus varies with the ecological strategies of bacteria. J Bacteriol 189:3237–3245. https://doi.org/10.1128/JB.01686-06.

64. Saifuddin M, Bhatnagar JM, Segrè D, Finzi AC. 2019. Microbial carbon use efficiency predicted from genome-scale metabolic models. Nat Commun 10:3568. https://doi.org/10.1038/s41467-019-11488-z.

65. Xu B, Sun Q-J, Lan JC-W, Chen W-M, Hsueh C-C, Chen B-Y. 2019. Exploring the glyphosate-degrading characteristics of a newly isolated, highly adapted indigenous bacterial strain, Providencia rettgeri GDB 1. J Biosci Bioeng 128:80–87. https://doi.org/10.1016/j.jbiosc.2019.01.012.

66. Dawes EA, Ribbons DW. 1964. Some aspects of the endogenous metabolism of bacteria. Bacteriol Rev 28:126–149. https://doi.org/10.1128/MMBR.28.2.126-149.1964.

67. Fahey TJ, Yavitt JB, Sherman RE, Groffman PM, Fisk MC, Maerz JC. 2011. Transport of carbon and nitrogen between litter and soil organic matter in a northern hardwood forest. Ecosystems 14:326–340. https://doi.org/10.1007/s10021-011-9414-1.

68. Goodale CL, Fredriksen G, Weiss MS, McCalley CK, Sparks JP, Thomas SA. 2015. Soil processes drive seasonal variation in retention of 15N tracers in a deciduous forest catchment. Ecology 96:2653–2668. https://doi.org/10.1890/14-1852.1.

69. Dabek-Szreniawska M, Hattori T. 1981. Winogradsky's salts solution as a diluting medium for plate count of oligotrophic bacteria in soil. J Gen Appl Microbiol 27:517–518. https://doi.org/10.2323/jgam.27.517.

70. Griffiths RI, Whiteley AS, O'Donnell AG, Bailey MJ. 2000. Rapid method for coextraction of DNA and RNA from natural environments for analysis of ribosomal DNA- and rRNA-based microbial community composition. Appl Environ Microbiol 66:5488–5491. https://doi.org/10.1128/aem.66.12.5488-5491.2000.

71. Bolger AM, Lohse M, Usadel B. 2014. Trimmomatic: a flexible trimmer for Illumina sequence data. Bioinformatics 30:2114–2120. https://doi.org/10.1093/bioinformatics/btu170.

72. Gordon A, Hannon G. 2010. Fastx-toolkit. FASTQ/A short-reads preprocessing tools. http://hannonlab.cshl.edu/fastx_toolkit.

73. Bankevich A, Nurk S, Antipov D, Gurevich AA, Dvorkin M, Kulikov AS, Lesin VM, Nikolenko SI, Pham S, Prjibelski AD, Pyshkin AV, Sirotkin AV, Vyahhi N, Tesler G, Alekseyev MA, Pevzner PA. 2012. SPAdes: a new genome assembly algorithm and its applications to single-cell sequencing. J Comput Biol 19:455–477. https://doi.org/10.1089/cmb.2012.0021.

74. Hyatt D, Chen G-L, LoCascio PF, Land ML, Larimer FW, Hauser LJ. 2010. Prodigal: prokaryotic gene recognition and translation initiation site identification. BMC Bioinformatics 11:119. https://doi.org/10.1186/1471-2105-11-119.

75. Arkin AP, Cottingham RW, Henry CS, Harris NL, Stevens RL, Maslov S, Dehal P, Ware D, Perez F, Canon S, Sneddon MW, Henderson ML, Riehl WJ, Murphy-Olson D, Chan SY, Kamimura RT, Kumari S, Drake MM, Brettin TS, Glass EM, Chivian D, Gunter D, Weston DJ, Allen BH, Baumohl J, Best AA, Bowen B, Brenner SE, Bun CC, Chandonia J-M, Chia J-M, Colasanti R, Conrad N, Davis JJ, Davison BH, DeJongh M, Devoid S, Dietrich E, Dubchak I, Edirisinghe JN, Fang G, Faria JP, Frybarger PM, Gerlach W, Gerstein M, Greiner A, Gurtowski J, Haun HL, He F, Jain R, et al. 2018. KBase: the United States department of energy systems biology knowledgebase. Nat Biotechnol 36:566–569. https://doi.org/10.1038/nbt.4163.

76. Price MN, Dehal PS, Arkin AP. 2010. FastTree 2—approximately maximum-likelihood trees for large alignments. PLoS One 5:e9490. https://doi.org/10.1371/journal.pone.0009490.

77. Aziz RK, Bartels D, Best AA, DeJongh M, Disz T, Edwards RA, Formsma K, Gerdes S, Glass EM, Kubal M, Meyer F, Olsen GJ, Olson R, Osterman AL, Overbeek RA, McNeil LK, Paarmann D, Paczian T, Parrello B, Pusch GD, Reich C, Stevens R, Vassieva O, Vonstein V, Wilke A, Zagnitko O. 2008. The RAST Server: Rapid Annotations using Subsystems Technology. BMC Genomics 9:75. https://doi.org/10.1186/1471-2164-9-75.

78. Kruger NJ. 2009. The Bradford method for protein quantitation, p 17–24. *In* Walker JM (ed), The protein protocols handbook. Humana Press, Totowa, NJ. https://doi.org/10.1007/978-1-59745-198-7_4.

79. Myklestad SM, Skånøy E, Hestmann S. 1997. A sensitive and rapid method for analysis of dissolved mono- and polysaccharides in seawater. Mar Chem 56:279–286. https://doi.org/10.1016/S0304-4203(96)00074-6.

80. Doane TA, Horwáth WR. 2003. Spectrophotometric determination of nitrate with a single reagent. Anal Lett 36:2713–2722. https://doi.org/10.1081/AL-120024647.

81. Miranda KM, Espey MG, Wink DA. 2001. A rapid, simple spectrophotometric method for simultaneous detection of nitrate and nitrite. Nitric Oxide 5:62–71. https://doi.org/10.1006/niox.2000.0319.

82. Rhine ED, Mulvaney RL, Pratt EJ, Sims GK. 1998. Improving the Berthelot reaction for determining ammonium in soil extracts and water. Soil Sci Soc Am J 62:473–480. https://doi.org/10.2136/sssaj1998.03615995006200020026x.

83. Joergensen RG. 1996. Quantification of the microbial biomass by determining ninhydrin-reactive N. Soil Biol Biochem 28:301–306. https://doi.org/10.1016/0038-0717(95)00141-7.

84. Jones DL, Owen AG, Farrar JF. 2002. Simple method to enable the high resolution determination of total free amino acids in soil solutions and

soil extracts. Soil Biol Biochem 34:1893–1902. https://doi.org/10.1016/S0038-0717(02)00203-1.

85. Moore S, Stein WH. 1948. Photometric ninhydrin method for use in the chromatography of amino acids. J Biol Chem 176:367–388.

86. Hochgräfe F, Wolf C, Fuchs S, Liebeke M, Lalk M, Engelmann S, Hecker M. 2008. Nitric oxide stress induces different responses but mediates comparable protein thiol protection in *Bacillus subtilis* and *Staphylococcus aureus*. J Bacteriol 190:4997–5008. https://doi.org/10.1128/JB.01846-07.

87. Simpson MJ, McKelvie JR. 2009. Environmental metabolomics: new insights into earthworm ecotoxicity and contaminant bioavailability in soil. Anal Bioanal Chem 394:137–149. https://doi.org/10.1007/s00216-009-2612-4.

88. Aristilde L, Reed ML, Wilkes RA, Youngster T, Kukurugya MA, Katz V, Sasaki CRS. 2017. Glyphosate-induced specific and widespread perturbations in the metabolome of soil Pseudomonas species. Front Environ Sci 5:34. https://doi.org/10.3389/fenvs.2017.00034.

89. Lu W, Clasquin MF, Melamud E, Amador-Noguez D, Caudy AA, Rabinowitz JD. 2010. Metabolomic analysis via reversed-phase ion-pairing liquid chromatography coupled to a stand alone orbitrap mass spectrometer. Anal Chem 82:3212–3221. https://doi.org/10.1021/ac902837x.

90. Klein AR, Barzen-Hanson KA, Aristilde L. 2020. A non-derivatized method for simultaneous quantitation of proteinogenic, urea-cycle, and acetylated amino acids by liquid chromatography–high-resolution mass spectrometry. Environ Chem Lett 18:229–235. https://doi.org/10.1007/s10311-019-00927-4.

91. Tautenhahn R, Patti GJ, Rinehart D, Siuzdak G. 2012. XCMS Online: a web-based platform to process untargeted metabolomic data. Anal Chem 84:5035–5039. https://doi.org/10.1021/ac300698c.

92. R Core Team. 2019. R: a language and environment for statistical computing. R Foundation for Statistical Computing, Vienna, Austria.

93. Sumner LW, Amberg A, Barrett D, Beale MH, Beger R, Daykin CA, Fan TW-M, Fiehn O, Goodacre R, Griffin JL, Hankemeier T, Hardy N, Harnly J, Higashi R, Kopka J, Lane AN, Lindon JC, Marriott P, Nicholls AW, Reily MD, Thaden JJ, Viant MR. 2007. Proposed minimum reporting standards for chemical analysis. Metabolomics 3:211–221. https://doi.org/10.1007/s11306-007-0082-2.

94. Djoumbou Feunang Y, Eisner R, Knox C, Chepelev L, Hastings J, Owen G, Fahy E, Steinbeck C, Subramanian S, Bolton E, Greiner R, Wishart DS. 2016. ClassyFire: automated chemical classification with a comprehensive, computable taxonomy. J Cheminform 8:61. https://doi.org/10.1186/s13321-016-0174-y.

95. Padfield D, Matheson G. 2018. nls.multstart: robust non-linear regression using AIC scores. https://CRAN.R-project.org/package=nls.multstart.

96. Petzoldt T. 2018. growthrates: estimate growth rates from experimental data. https://CRAN.R-project.org/package=growthrates.

97. Haug K, Cochrane K, Nainala VC, Williams M, Chang J, Jayaseelan KV, O'Donovan C. 2020. MetaboLights: a resource evolving in response to the needs of its scientific community. Nucleic Acids Res 48:D440–D444. https://doi.org/10.1093/nar/gkz1019.